Experimental Study of Heating Surface Angle Effects on Single Bubble Growth

Jeongbae Kim*
New & Renewable Energy Research Department,
KIER (Korea Institute of Energy Research),
71-2, Jang-dong, Yuseong-gu, Daejeon 305-343, Korea
Hyung Dae Kim
Department of Mechanical Engineering, Pohang University of Science and Technology,
San 31, Hyoja-dong, Namgu, Pohang, Kyoungbuk 790-784, Korea
Jangho Lee
Department of Mechanical Engineering, Kunsan National University,
San 68, Miryong-dong, Kunsan, Jellabuk-do 573-701, Korea
Young Chul Kwon
Division of Mechanical Engineering, Sunmoon University,
100, Kalsan-ri, Tangjeong-myeon, Asan, ChungNam-do 336-708, Korea
Jeong Hoon Kim
Department of Mechanical Engineering, Pusan National University,
San 30, Jangjeon-dong, Geomjeong-gu, Busan 609-735, Korea
Moo Hwan Kim
Department of Mechanical Engineering, Pohang University of Science and Technology,
San 31, Hyoja-dong, Namgu, Pohang, Kyoungbuk 790-784, Korea

Nucleate pool boiling experiments were performed using pure R11 for various surface angles under constant heat flux conditions during saturated pool boiling. A 1-mm-diameter circular heater with an artificial cavity in the center that was fabricated using a MEMS technique and a high-speed controller were used to maintain the constant heat flux. Bubble growth images were taken at 5000 frames per second using a high-speed CCD camera. The bubble geometry was obtained from the captured bubble images. The effects of the surface angle on the bubble growth behavior were analyzed for the initial and thermal growth regions using dimensional scales. The parameters that affected the bubble growth behavior were the bubble radius, bubble growth rate, sliding velocity, bubble shape, and advancing and receding contact angles. These phenomena require further analysis for various surface angles and the obtained constant heat flux data provide a good foundation for such future work.

Key Words : Surface Angle, Constant Heat Flux, Single Bubble Growth, Nucleate Pool Boiling, Circular Heater, Artificial Cavity

* Corresponding Author,
E-mail : doctorkjb@kier.re.kr
TEL : +82-42-860-3569; **FAX** : +82-42-860-3538
New & Renewable Energy Research Department, KIER (Korea Institute of Energy Research), 71-2, Jang-dong, Yuseong-gu, Daejeon 305-343, Korea. (Manuscript **Received** March 21, 2006; **Revised** August 30, 2006)

Nomenclature

A : Dimensional parameter for bubble volume calculations
A_b : Dimensional parameter for the characteristic bubble scale
B : Dimensional parameter for bubble vol-

ume calculations
B_b : Dimensional parameter for the characteristic bubble scale
C : Dimensional parameter for bubble volume calculations
C_{P_l} : Liquid specific heat
D : Dimensional parameter for bubble volume calculations
E : Dimensional parameter for bubble volume calculations
F : Dimensional parameter for bubble volume calculations
h_{fg} : Latent heat of vaporization
Ja : Jakob number, defined by $(\rho_l C_{P_l} \Delta T)/(\rho_v h_{fg})$
$\dot{m}$: Evaporating mass flow rate
$\dot{q}$: Heat flow rate
R^+ : Dimensionless radius
$(R^+)_d$: Dimensionless radius based on departure radius
R : Radius or equivalent bubble radius
R_{ch} : Characteristic bubble radius scale
R_d : Departure bubble radius
t : Time
t_{ch} : Characteristic timescale
t^+ : Dimensionless time
$(t^+)_d$: Dimensionless time based on departure time
T_{sat} : Saturation temperature
T_{wall} : Wall temperature
V : Total bubble volume
V_L : Bubble volume of the lower part
V_U : Bubble volume of the upper part

Greek Symbols

α_l : Liquid thermal diffusivity
ΔT : Wall superheat, defined by $T_{wall} - T_{sat}$
ρ_v : Vapor density
ρ_l : Liquid density

1. Introduction

The bubble radius results of Han and Griffith (1965) and Cole and Shulman (1966), performed at constant heat flux conditions during saturated pool boiling, contained large deviations, even when the tests were performed under the same experimental conditions. These deviations arose from the poor control capacity of the heating surface. Lee et al.(2003) showed that the control speed of the heating surface must be only a few microseconds to maintain constant heating conditions from bubble inception to departure.

Lee et al.(2003) reported that the bubble growth rate in the thermal growth region varied with $t^{1/7}$ when only one wall superheat condition occurred during saturated pool boiling using R11. The initial growth rate varied with t^1, as proposed by Rayleigh (1917). For various wall superheats, Lee et al.(2003) demonstrated that the bubble growth rate in the thermal growth region varied with $t^{1/5}$ during saturated pool conditions using R11 and R113; however, the initial growth rate still varied with t^1. They used a Jakob number (Ja) based on the wall superheat (the difference between the wall and saturation temperatures) ranging from 14 to 21. They also reported that the thermal growth rate was independent of the working fluid and heating conditions. Lee et al. (2004) showed that the growth behavior of binary mixtures in the thermal growth region during saturated pool conditions was almost identical to that of pure substances. Kim et al.(2006) performed nucleate pool boiling experiments with fixed wall temperatures using one fluid to examine pool temperature effects on the bubble growth behavior under constant atmospheric pressure conditions. They showed that the bubble radius was proportional to between $t^{1/2}$ and $t^{2/3}$ in the initial growth region and proportional to $t^{1/5}$ in the thermal growth region, regardless of the heating conditions, under saturated pool conditions. All these single bubble growth results were acquired with a horizontal heating surface under saturated pool conditions, except for Rayleigh's (1917) analysis.

Many studies have investigated the effects of the surface angle on pool boiling. Githinji and Sabersky (1963) analyzed the effects of the surface angle during nucleate boiling. They made comparisons of the boiling heat transfer from a 0.3-cm-wide strip in isopropyl alcohol for three different surface angles: horizontal facing up-

ward, vertical, and horizontal facing downward. They observed that the boiling curve for the horizontal strip facing downward differed significantly from those for the other angles. Chen (1978) conducted similar pool boiling experiments in R11 using a 3.7×2.5-cm copper plate. He concluded that the heat transfer coefficient at a given wall superheat increased as the inclination angle increased from 0° (horizontal facing upward) to about 150° (inclined facing downward by 30°), and dropped rapidly to a minimum value at 180° (horizontal facing downward). The angular dependence of the nucleate pool boiling heat transfer coefficient for a plain surface was also reported by Jung et al.(1987) and Chang and You (1996). Rainey and Yoo (2001) experimentally examined the effects of the heater size and surface angle during pool boiling from nucleate to critical heat flux (CHF) between plain and coated surfaces. Although they focused on the effects of the surface angle on the CHF behavior, they also demonstrated that the nucleate pool boiling characteristics differed for various surface angles.

To our knowledge, no study has reported the surface angle effects for a plain surface with an onset of nucleate boiling (ONB) heat flux and single bubble growth behavior during nucleate heat transfer. When analyzing the effect of the heating surface angle on the bubble growth, one must consider the bubble sliding along the surface, how much the angle affects the bubble growth rate, and the difference between the single bubble growth rate and that obtained for boiling flow at a low Reynolds number.

The objective of this study was to analyze single bubble growth behavior at an ONB heat flux under saturated pool conditions and atmospheric pressure. To achieve our objective, nucleate pool boiling tests were conducted for saturated pool conditions (pool temperature : 24.0℃) using pure R11 (saturation temperature : 23.7℃). The wall heat flux was maintained at 13.6 kW/m^2 for all surface angles, using a 1-mm-diameter circular heater and a high-speed controller, to investigate the effect of only the surface angle on the single bubble growth characteristics. These included the bubble growth rate during the initial and thermal growth regions. The surface angles were set to 0°, 30°, 60°, and 90° (measured horizontally upwards, counterclockwise) to consider the horizontal and vertical heating conditions that are often applied in actual heating situations. The heat fluxes at the ONB points at all surface angles were also measured throughout this study.

2. Experiments

2.1 Apparatus

We used a circular heater to maintain a constant heat flux at the heating surface. The heater was fabricated on a transparent glass wafer using a very large-scale integrated (VLSI) technique. The transparency provided a bottom view of the growing bubble, which was captured using a high-speed CCD camera. First, a titanium and platinum layer for the heater line was installed on the wafer using thermal evaporation. Then, a titanium and platinum layer for the power line was fabricated. The roughness of the heating surface was approximately 0.4 μm, which was the height of the heating line with respect to the base substrate. The width of the heating line was 10 μm and the distance between the heating lines was also 10 μm.

The static contact angle of the platinum surface was 71° for distilled water and 11.4° for R113, which indicates the hydrophilic nature of R113. The diameter of the circular heater was 1 mm. The cylindrical artificial cavity, 14.5 μm in diameter and 35 μm in depth, was manufactured at the center of the heater. The distance from the cavity to the left heater line was 15 μm and the length from the cavity to the right heater line was 18 μm. The electrical resistance of the heater was 8.404 kΩ. When the connector for the power supply was included, this resistance increased to 8.414 kΩ. The heater was manufactured by a MEMS fabrication company using a method based on the idea of Rule et al.(1998) and Rule and Kim (1999). Figure 1 shows a schematic diagram of the circular heater.

A constant heat flux condition was achieved by controlling the DC voltage supplied to the heater. The voltage data were measured and sto-

red at 100 kHz, and controlled to less than ±2% of a fixed 9.5 V throughout the tests. Figure 2 shows a schematic diagram of the experimental apparatus. A 150-W cold light source was used for the CCD camera (Redlake Co., HG-100 K), which had a speed of 5000 frames per second. A long-distance microscopic lens was used to capture the small bubbles during boiling.

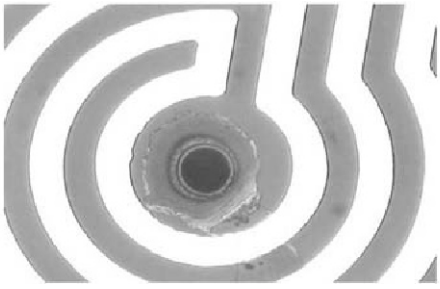

(a) Artificial cavity structure

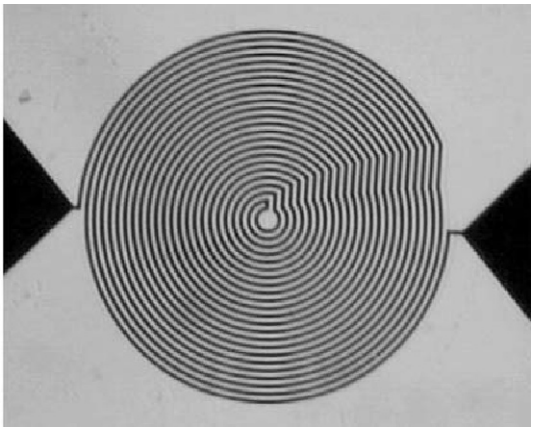

(b) Circular heater

Fig. 1 Schematic diagram of the circular heater

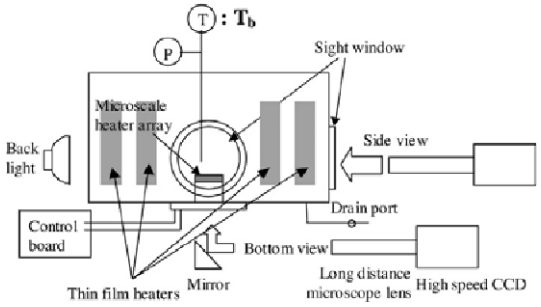

Fig. 2 Schematic diagram of the experimental apparatus

2.2. Uncertainty analysis

The bubble growth behavior was analyzed using side-view images during growth. Since most of the previous results for bubble growth have been for a spherical bubble, the growth behavior in this study was analyzed using the equivalent radius of a sphere with the same volume. The captured images showed asymmetric bubble geometries, both about the vertical and horizontal axes, except for a surface angle of 0°. Based on our shape assumption, illustrated in Fig. 3, we calculated the volume of the upper left, upper right, lower left, and lower right parts of the bubble using

$$V_{UL}=\frac{2}{3}\pi A_L^2 E_L\times\frac{1}{2} \tag{1}$$

$$V_{UR}=\frac{2}{3}\pi A_R^2 E_R\times\frac{1}{2} \tag{2}$$

$$V_{LL}=\pi A_L^2\left[D_L-\frac{{D_L}^3}{3F_L^2}\right],\ F_L=\sqrt{\frac{D_L^2}{1-\frac{C_L^2}{{A_L}^2}}} \tag{3}$$

$$V_{LR}=\pi A_R^2\left[D_L-\frac{{D_R}^3}{3F_R^2}\right],\ F_R=\sqrt{\frac{D_R^2}{1-\frac{C_R^2}{{A_R}^2}}} \tag{4}$$

where A, A_R, A_L, B, D_R, D_L, E_R, E_L, C, C_R, C_L, F_R, and F_L are the dimensions indicated in

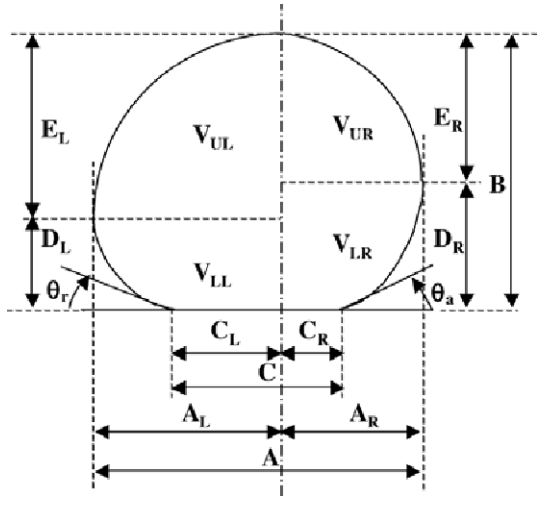

Fig. 3 Geometry used to determine the bubble volume

Fig. 3 and the horizontal and vertical lengths are measured from the top point of the bubble. V_{UL} is the volume of the upper left part of the bubble, V_{UR} is the volume of the upper right part of the bubble, V_{LL} is the volume of the lower left part of the bubble, and V_{LR} is the volume of the lower right part of the bubble. Thus, V_U and V_L can be calculated by summing V_{UL} with V_{UR} and V_{LL} with V_{LR}. The equivalent radius, R_{eq}, can then be defined as the radius for which the total volume (V) from the measurements is balanced with that of a sphere with an equivalent radius :

$$V = V_U + V_L = \frac{4}{3}\pi R_{eq}{}^3 = \frac{4}{3}\pi R^3 \qquad (5)$$

The equivalent radius can be calculated from the bubble dimensions using Eqs. (1) ~ (5). However, any errors in the dimensional measurements will be propagated in the calculations. The bubble dimensions were measured by counting the number of pixels in each captured image. A micrometer was placed in the chamber at the same distance as the bubble nucleation to provide guidance for the size measurements. From the captured micrometer images, a physical dimension of 1000 μm corresponded to 147 pixels in our tests. Therefore, one pixel in each image corresponded to 6.8027 μm. The clearly captured images could be measured with an error of ± 1 pixel. An uncertainty analysis was performed using the method described by Coleman and Steele (1989). The maximum uncertainty in the first image, which contained the smallest bubble, was about 6.0%.

3. Results and Discussion

3.1 ONB for various surface angles

To demonstrate the capabilities of our heater, we measured the ONB heat flux for various surface angles. The ONB heat flux increased with the surface angle, as reported in other studies including Rainey and You (2001) (see Fig. 4). The heat fluxes at the ONB were 10.80, 12.34, 12.56, and 12.75 kW/m^2 for surface angles of 0°, 30°, 60°, and 90°, respectively. The ONB heat flux for 0°, 10.80 kW/m^2, was much less than that reported by Lee et al. (2003), 234.96 kW/m^2, due to the presence of the artificial cavity in our heater.

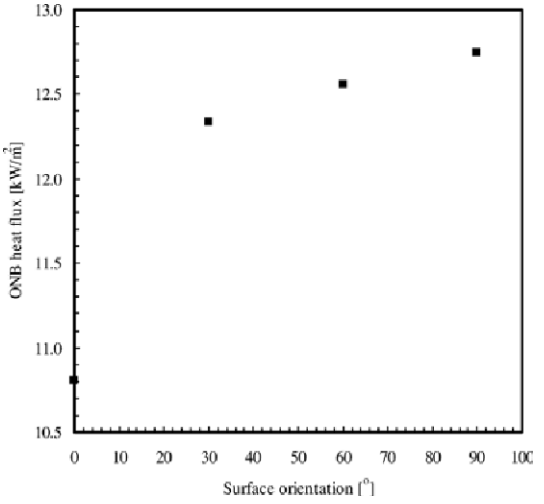

Fig. 4 ONB heat flux for different surface angles

3.2 Bubble growth and departure behavior

To achieve our objective, single bubble tests during nucleate pool boiling were conducted at saturated pool conditions using pure R11. We analyzed the bubble shapes during growth using the captured image, such as those shown in Fig. 5, to verify that the assumed bubble geometry used to obtain the equivalent bubble radius was reasonable. The images showed bubbles that were symmetric neither about the axis normal to the heating surface nor about the horizontal axis, except when the surface angle was 0°. The images for 0° showed bubbles that were almost symmetric about the axis normal to the heating surface but not symmetric about the horizontal axis, as expected.

The bubble radius obtained in this study for a surface angle of zero degrees was much smaller than those reported by Lee et al. (2003), which used the same fluid and pool conditions (see Fig. 6(a)). The bubble radius was affected by the heat flux difference between the two experiments, as described above, but the dimensionless bubble radius behavior was similar (see Fig. 6(b)). The dimensionless bubble radius $(R^+)_d$ and time $(t^+)_d$ can be calculated from the departure radius (R_d) and time (t_d) as

$$(R^+)_d=\frac{R}{R_d},\ (t^+)_d=\frac{t}{t_d} \tag{6}$$

The growth rate in the initial growth region at saturated pool conditions with a surface angle of 0° was proportional to $t^{1/2}$, which is slightly less than $t^{2/3}$ proposed by Kim et al.(2006), and

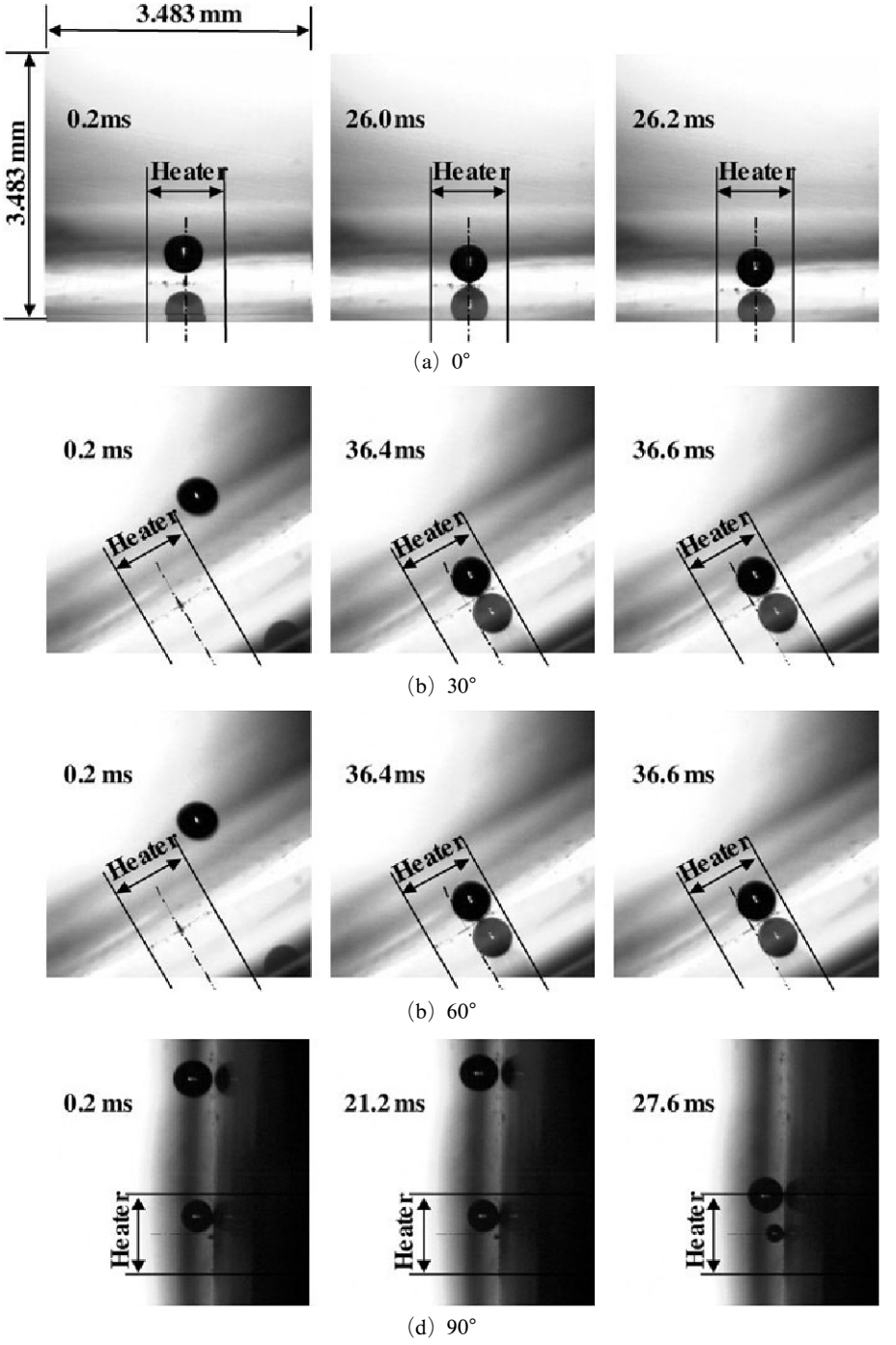

Fig. 5 Side view images of the bubble growth

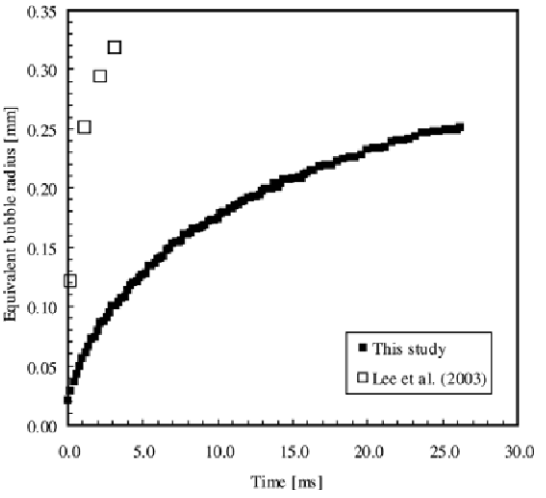

(a) Bubble radius comparison (dimensional scale)

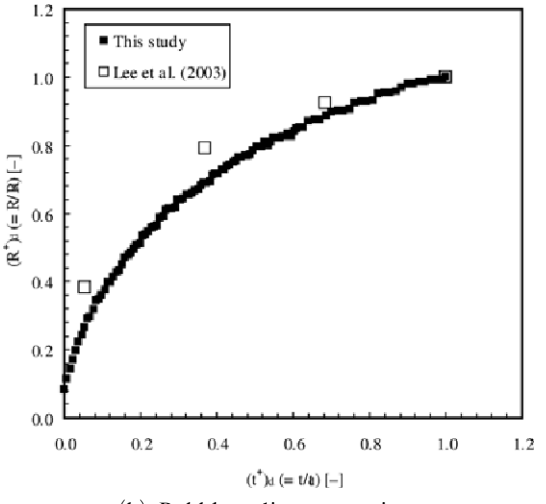

(b) Bubble radius comparison (nondimensional scale)

Fig. 6 Comparison of the bubble growth behavior at a surface angle of 0°

the growth rate in the thermal growth region was proportional to t0.226, which is the same as previous results (see Fig. 7). The departure and waiting times were 26.2 and 3.8 ms, respectively. Compared to the results of Lee et al.(2003), the departure time was longer due to the smaller heat flux and the waiting time was shorter due to the larger cavity size. The cavity diameter in the present study was 14.5 μm, while that of Lee et al. (2003) was an estimated 0.567 μm. The power of time for the bubble growth is intimately related to

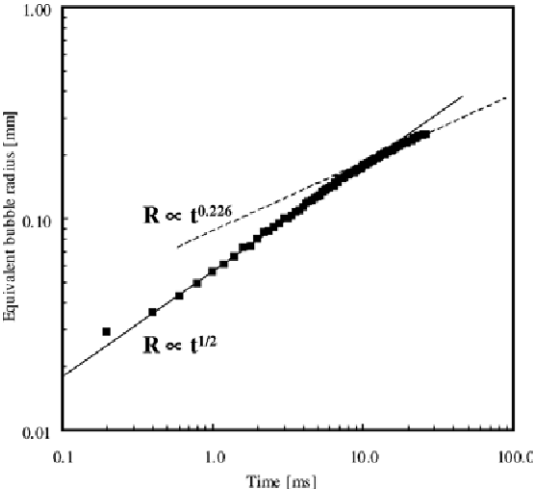

Fig. 7 Bubble growth behavior at a surface angle of 0°

the heat flow rate behavior. If the power of time for the bubble growth is less than one-third, the heat flow rate described by Eq. (7) will decrease. Therefore, the heat flow rate increased with time during the initial growth region when the power of the growth rate was 0.5 and decreased with time during the thermal growth region when the power of the growth rate was 0.226 (see Fig. 7), as proposed by previous studies.

The rate of heat flow supplied to the bubble corresponds to the required energy for the total bubble volume change based on the assumption that the volume change is induced by the latent heat transfer. This can be calculated from

$$\dot{q}=\dot{m}h_{fg}=4\pi\rho_v h_{fg}R^2\frac{dR}{dt} \qquad (1)$$

where $\dot{q}$ is the heat flow rate, $\dot{m}$ is the evaporating mass flow rate, h_{fg} is the latent heat of vaporization, ρ_v is the vapor density, R is the equivalent bubble radius, and t is time.

The bubble growth behaviors for surface angles of 30°, 60°, and 90° were different from that obtained for a surface angle of 0° since the bubble slid along the surface, as shown in Fig. 5(b) and (d). For a surface angle of 30°, the initial growth rate was almost the same as that obtained for a horizontal surface, but the thermal growth rate increased to $t^{0.381}$ due to the difference in the thermal boundary layer near the bubble caused

by the sliding, which creates conditions similar to forced convective heat transfer (see Fig. 8). The bubble strayed out of the artificial cavity after 25.8 ms and departed from the heater after 36.6 ms. The initial growth behavior was very different when the surface angle was 60°. Another single bubble formed in the cavity after 25.0 ms while the preceding bubble still was attached to the heating surface. The growth rate in the early stages of the initial growth region was $t^{0.341}$, less than that obtained for a surface angle of 0° or 30°; this increased to $t^{0.484}$ in the later stages of the initial growth region after the departure of the proceeding bubble. The growth rate in the thermal growth region was $t^{0.434}$, which is higher than that obtained for a surface angle of 0° or 30°. The departure occurred inside the heater. The bubble strayed out of the artificial cavity after 18.0 ms and departed from the heater after 26.6 ms (see Fig. 9). The initial growth behavior was similar when the surface angle increased from 60° to 90°. Again, another single bubble was formed in the cavity while the preceding bubble was still attached to the heating surface. At a surface angle of 90°, the growth rate in the early stages of the initial growth region was $t^{0.348}$. This increased to $t^{0.460}$ after the departure of the proceeding bubble. The growth rate in the thermal growth region was $t^{0.444}$, which was higher than that obtained for a surface angle of 0°, 30°, or 60°. The first departure occurred outside of the heater, but then the bubble reattached after sliding a distance of 30.6 ms and departed from the surface again after 37.8 ms. The bubble strayed out of the artificial cavity after 13.6 ms, left the heater after 27.0 ms, and departed from the surface for the first time after 27.6 ms (see Fig. 10).

The estimated equivalent bubble radii for each surface angle are shown in Fig. 11. At a given instant in time, the bubble radius for an inclined

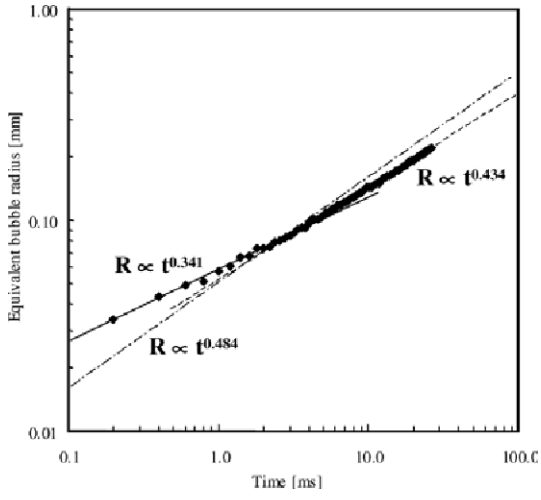

Fig. 9 Bubble growth behavior at a surface angle of 60°

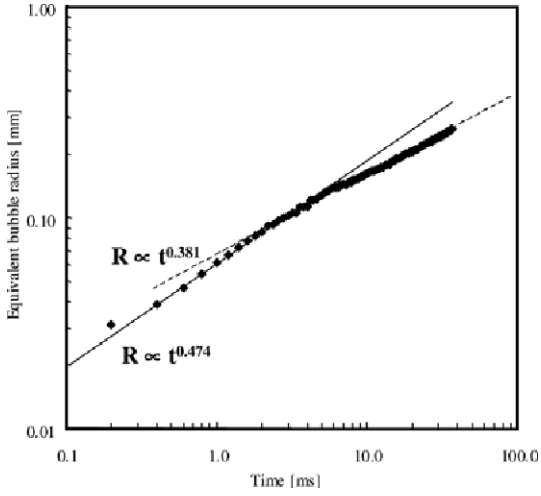

Fig. 8 Bubble growth behavior at a surface angle of 30°

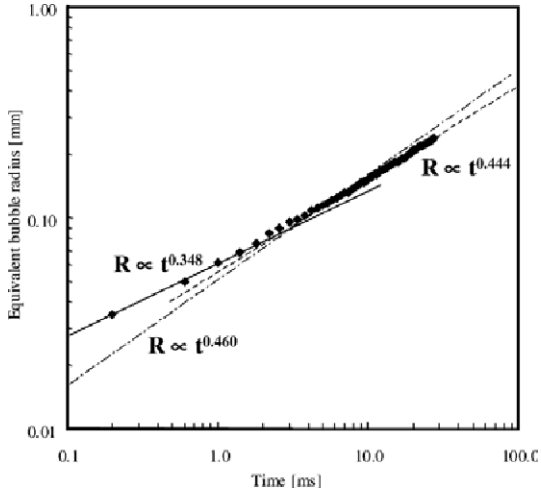

Fig. 10 Bubble growth behavior at a surface angle of 90°

heating surface was less than that obtained for the horizontal heating surface. But while larger bubbles were formed as the surface angle increased from 0° to 60°, the bubble size decreased when the surface angle increased from 60° to 90°. It is well known that the bubble size is affected by changes in the thermal boundary layer and flow characteristics when the bubble slides under the same inception conditions. Further analyses or experiments are required using various surface angles and considering other surface conditions, including constant surface temperatures and variable surface energies, to clearly illustrate these phenomena. The observed bubble growth and departing behaviors for various surface angles are summarized in Table 1.

3.3 Bubble sliding behavior

To estimate the sliding length and velocity from the captured bubble images, a reference location was fixed to the heater (or cavity) center. The sliding length was calculated as the distance from the heater center to the center of the contact length, and the sliding velocity was acquired from the sliding length divided by the time from inception. However, a sharp increase in the sliding velocity right after inception occurred, as shown in Fig.

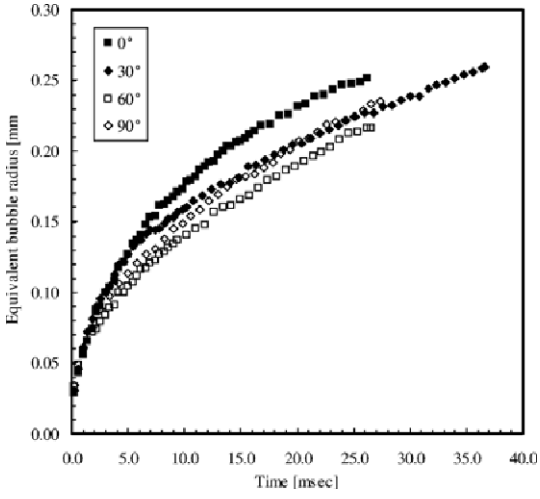

Fig. 11 Equivalent bubble radius for different surface angles

Table 1 Bubble growth and departure characteristics for various surface angles

Surface angle [°]	0	30	60	90
Bubbles on the heater at inception	1	1	2	2
Sliding	no	yes	yes	yes
Proceeding bubble departure time (ms)	—	—	3.0	5.6
Time to leave cavity (ms)	—	25.8	18.0	13.6
Time to leave heater (ms)	—	—	—	27.0
Departure time (ms)	26.1	36.6	26.6	27.6
Next bubble incepted (ms)	29.9	46.4	25.0	21.2
Reattach to surface (ms)	—	—	—	30.6
Second deqarture (ms)	—	—	—	37.8

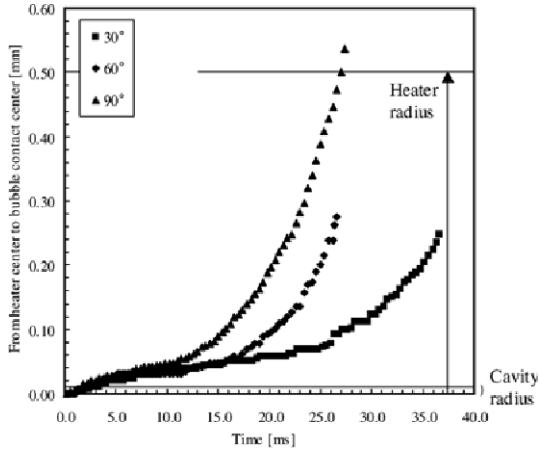

(a) Length from heater center to bubble contact center

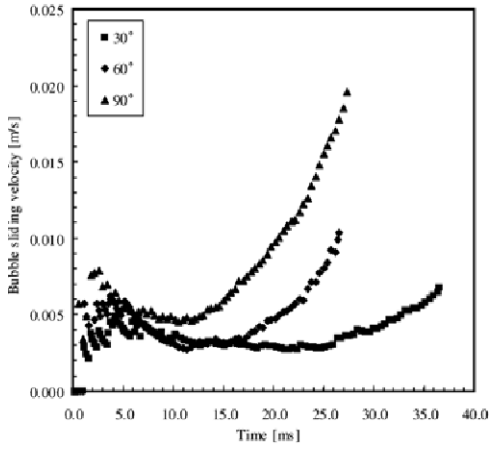

(b) Bubble sliding velocity from bubble inception

Fig. 12 Bubble sliding characteristics for various surface angles

12(b), resulting from pixel errors and the small time duration. As expected, the bubble sliding velocity was higher for larger surface angles. As described above, when the surface angle was 90°, the departure occurred outside the heater, followed by a reattachment after 0.78 mm of sliding over 30.6 ms. The bubble departed a second time at 1.47 mm after 37.8 ms. When departing, the bubble sliding Reynolds number was calculated using the bubble sliding velocity and the equivalent bubble diameter as the characteristic velocity and length scales. The Reynolds numbers at departure were 2.034, 2.590, and 5.314 for surface angles of 30°, 60°, and 90°, respectively.

Lee et al.(2003) performed boiling flow experiments at Reynolds numbers of 2.9 and 8.3 using a single microchannel and demonstrated the behavior of single bubble growth. To compare the bubble growth during nucleate pool boiling with sliding and that during microchannel flow boiling, we examined the results of Lee et al.(2003) using the characteristic scales proposed by Mikic et al.(1970). The dimensionless radius and time were acquired from

$$R^+=\frac{R}{R_{ch}},\ t^+=\frac{t}{t_{ch}} \tag{8}$$

and the characteristic scales were

$$R_{ch}=B_{ch}^2/A_{ch},\ t_{ch}=B_{ch}^2/A_{ch}^2 \tag{9}$$

$$A_{ch}=\left[\frac{\pi}{7}\frac{\rho_v h_{fg}\Delta T}{\rho_l T_{sat}}\right]^{1/2},\ B_{ch}=\left[\frac{12}{\pi}\mathrm{Ja}^2\alpha_l\right]^{1/2} \tag{10}$$

As shown in Fig. 13, the single bubble growth rate in a single microchannel at a low Reynolds number gave $R^+\propto(t^+)^{0.379}$. The growth rate was greater than $t^{1/3}$ because the bubbles slid along the surface, and was almost same as the growth rates obtained during sliding in the present study when the surface angle was 30°, 60°, or 90°, except during the early stages of the initial growth region when two bubbles existed on the heating surface at the same time. This result demonstrates that sliding bubbles increase the heat transfer rate from the heating surface to the bubble.

Figure 14 shows the advancing contact angle

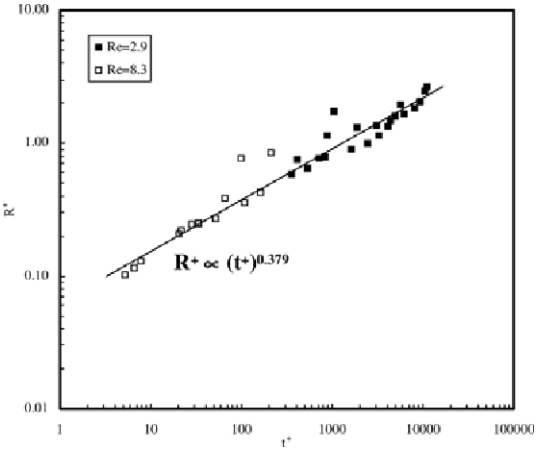

Fig. 13 Dimensionless bubble growth behavior for boiling flow at low Reynolds number

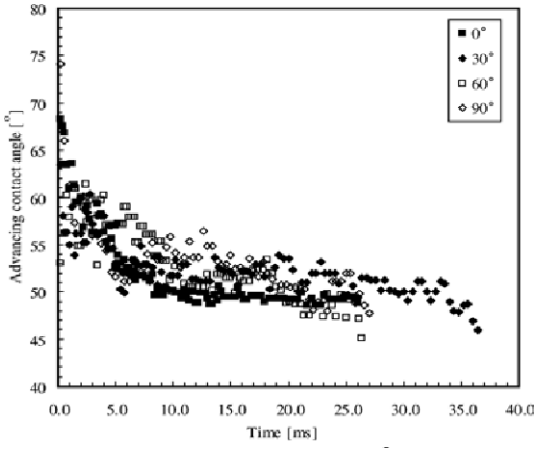

(a) Advancing contact angle (θ_a)

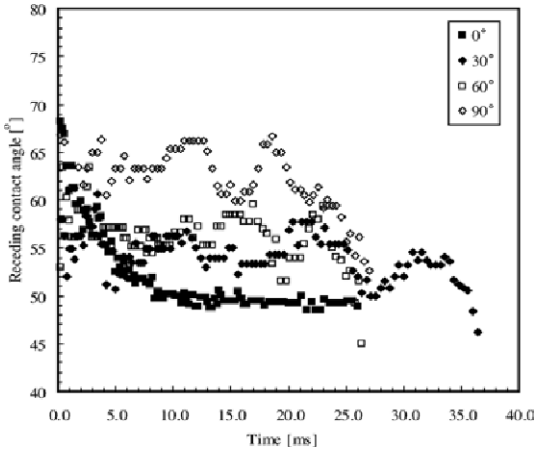

(b) Recceding contact angle (θ_r)

Fig. 14 Contact angles during growth

(ϑ_a) and receding contact angle (ϑ_r) as defined in Fig. 3. The advancing contact angles for surface angles of 30°, 60°, and 90° were similar to each other and greater than those obtained at a surface angle of 0°. The receding contact angle was generally larger for higher surface angles, but a significant variation was evident near the cavity mouth (see Fig. 14(b)).

3.4 Bubble geometry behavior

Figures 15 and 16 show the characteristics of the bubble geometry defined in Fig. 3 during the period of growth. The maximum bubble length (A) and bubble height (B) for all surface angles were similar to the bubble growth behavior (see Fig. 15). But similar to the behavior of the receding contact angle, large fluctuations in the bubble

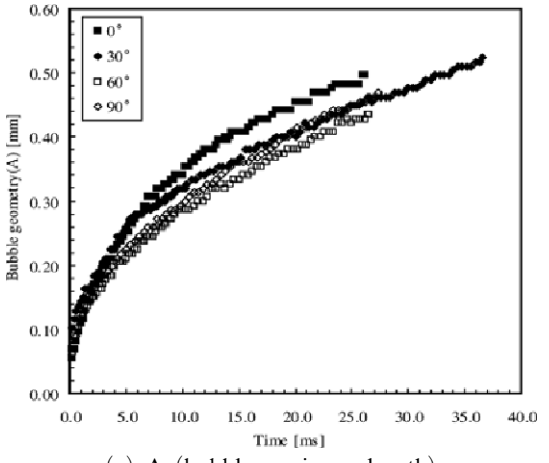

(a) A (bubble maximum length)

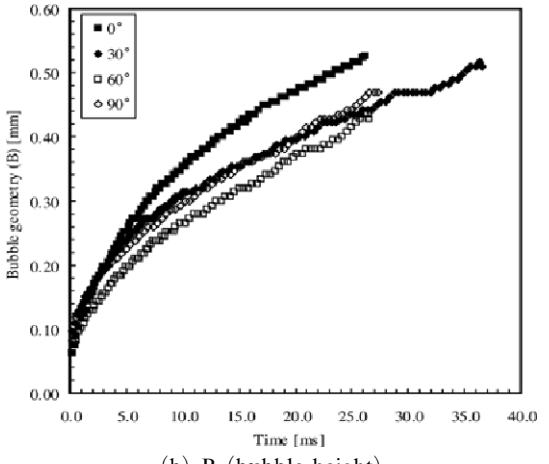

(b) B (bubble height)

Fig. 15 Bubble geometry (A and B) during growth

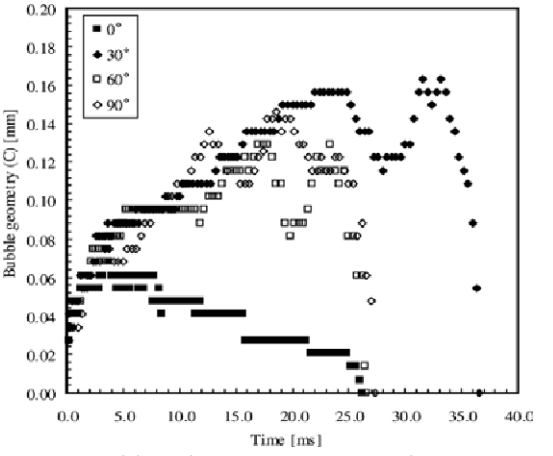

(a) C (bubble contact radius)

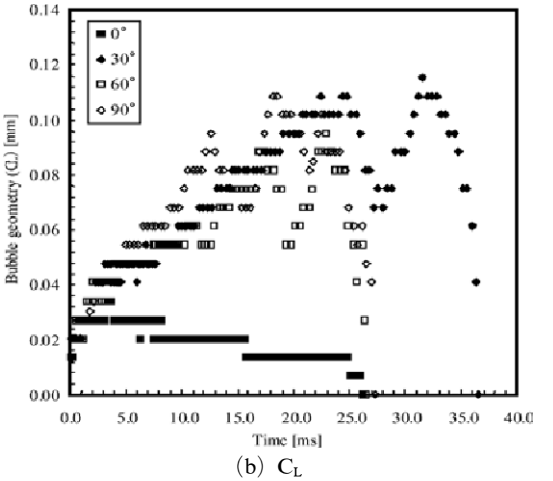

(b) C_L

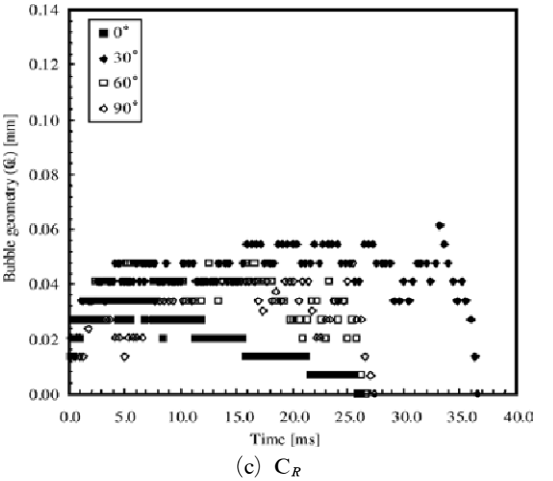

(c) C_R

Fig. 16 Bubble contact radius (C) during growth

contact radius (C) were observed near the cavity mouth during sliding (see Fig. 16).

4. Conclusions

The behavior of single bubbles during growth at various heating surface angles (0°, 30°, 60°, and 90°, measured counterclockwise from the horizontal axis) during saturated nucleate pool boiling was examined for a constant heat flux. Time-triggered high-speed CCD images were captured at a sampling rate of 5000 Hz to analyze the bubble motion. To perform the tests, we designed and used a circular platinum heater fabricated by a MEMS technique.

The heat flux characteristics at the ONB point were obtained for different surface angles. We used the equivalent radius of a sphere with the same volume as the slightly asymmetric bubbles in our calculations, which produced only a small error. We quantitatively determined the bubble growth rate and geometry for various heating surface angles with a fixed heat flux, and simultaneously calculated effect of the sliding length, sliding velocity, and advancing and receding contact angles. As expected, the bubble growth behavior was affected by changes in the thermal boundary layer near the bubble and the heating surface when the bubble slid along the surface. The simultaneous existence of the two bubbles at the heating surface, which occurred at surface angles of 60° and 90°, decreased the growth rate in the early stages of the initial growth region. The flow effects on sliding bubbles during pool boiling were similar to the bubble growth behavior in boiling flow at a low Reynolds number. The phenomena presented in this study require further analysis for various surface angles and the obtained constant heat flux data provide a good foundation for such future work.

References

Chang, J. Y. and You, S. M., 1996, "Heater Orientation Effects on Pool Boiling Micro-porous-enhanced Surfaces in Saturated FC-72," *ASME J. Heat Transfer*, Vol. 118, pp. 937～943.

Chen, L. T., 1978, "Heat Transfer to Pool Boiling Freon from Inclined Heating Plate," *Lett. Heat Mass Transfer*, Vol. 5, pp. 111～120.

Cole, R. and Shulman, H. L., 1966, "Bubble Growth Rates at High Jakob Numbers," *Int. J. Heat Mass Transfer*, Vol. 9, pp. 1377～1390.

Coleman, W. H. and Steele, W. G., 1989, "Experimentation and Uncertainty Analysis for Engineers," *John Wiley & Sons*.

Githinji, P. M. and Sabersky, R. H., 1963, "Some Effect of the Orientation of the Heating Surface in Nucleate Boiling," *ASME J. Heat Transfer*, Vol. 85, pp. 379.

Han, C. H. and Griffith, P., 1965, "The Mechanism of Heat Transfer in Nucleate Pool Boiling-Part I Bubble Initiation," *Growth and Departure, Int. J. Heat Mass Transfer*, Vol. 8, pp. 887～904.

Jung, D. S., Venart, J. E. S. and Sousa, A. C. M., 1987, "Effects of Enhanced Surfaces and Surface Orientation on Nucleate and Film Boiling Heat Transfer in R-11," *Int. J. Heat Mass Transfer*, Vol. 30, pp. 2627～2639.

Kim, J., Lee, J. and Kim, M. H., 2006, "Experimental Study on Single Bubble Growth under Subcooled, Saturated, and Superheated Nucleate Pool Boiling," *KSME Int. J.*, Vol. 20, No. 5, pp. 692～709f.

Lee, H. C., Kim, J., Oh, B. D. and Kim, M. H., 2004, "Single Bubble Growth in Saturated Pool Boiling of Binary Mixtues," *Int. J. of Multiphase Flow*, Vol. 30, No. 6, pp. 697～710.

Lee, H. C., Oh, B. D., Bae, S. W. and Kim, M. H., 2003, "Single Bubble Growth in Saturated Pool Boiling on a Constant Wall Temperature Surface," *Int. J. of Multiphase Flow*, Vol. 29, No. 12, pp. 1857～1874.

Lee, H. C., Oh, B. D., Bae, S. W., Kim, M. H., Lee, J. Y. and Song, I. S., 2003, "Partial Nucleate Boiling on the Microscale Heater Maintaining Constant Wall Temperature," *J. of Nuclear Science and Technology*, Vol. 40, No. 10, pp. 768～774.

Lee, J., Cho, K., Song, I. S., Kim, C. B. and Son, S. Y., 2003, "Microscale Bubble Nucleation from an Artificial Cavity in Single Microchannel," *ASME J. of Heat Transfer*, Vol. 125, pp. 545.

Mikic, B. B., Rohsenow, W. M. and Griffith, P., 1970, "On Bubble Growth Rates," *Int. J. Heat Mass Transfer*, Vol. 13, pp. 657～666.

Rainey, K. N. and You, S. M., 2001, "Effects of Heater Size and Orientation on Pool Boiling Heat Transfer from Microporous Coated Surfaces," *Int. J. Heat Mass Transfer*, Vol. 44, pp. 2589～2599.

Rayleigh, J. W. S., 1917, "On the Pressure Developed in a Liquid during the Collapse of a Spherical Cavity," *Philos. Mag*., Vol. 34, pp. 94～98. ; This is cited in the book titled "Boiling Phenomena" by S. Van Stralen (1979), McGraw-Hill.

Rule, T. D. and Kim, J., 1999, "Heat Transfer Behavior on Small Horizontal Heaters during Pool Boiling," *J. of Heat Transfer*, Vol. 121, No. 2, pp. 386～393.

Rule, T. D., Kim, J. and Kalkur, T. S., 1998, "Design, Construction and Qualification of a Microscale Heater Array for Use in Boiling Heat Transfer," NASA/CR-1998-207407.